

Chapter-3

Oxidation Behavior of Fe-18Cr-21Mn-0.65N Austenitic Stainless Steel

3.1. Introduction

Fe-Cr-Mn-N class of alloys are widely used as retainers' rings in power generators, drill collars of oil rigs, vessels of fusion bed reactors, and armor materials in defence sector. In nuclear industry, it is highly undesirable to use high nickel containing stainless steel because nickel in the steel undergoes activation by neutron radiation. This reduces ductility of the material in service and creates problems in disposal of components after decommissioning. In such applications, the Fe-Cr-Mn-N steel is cyclically exposed between 300-700°C. In several applications, this grade of stainless steel is welded with other low alloy steels and C-Mn steels and requires stress relieving after completion of welding [5-6]. Normally stress relieving temperature for low alloy C-Mn steel lies in the range of 500-700°C up to 10-40 h depending on thickness of the joint. Low temperature (400-500°C) stress relieving treatment of 8-10 h, is needed to remove peak stress and maintain dimensional stability during machining of stainless steel, however that, causes oxidation [7]. However, literature on the oxidation behavior of high Mn high nitrogen stainless steel with different airflow rates is scarce. Isothermal oxidation of Fe-Cr-Mn alloys in temperature range of 700-1000°C for 1500 h showed a higher oxidation rate than that of chromia forming alloys [86]. High chromium containing steels suffer from chromium vaporization during oxidation in the temperature range from 600-900°C in humid air at high flow rates [87]. The study on the effect of gas (wet air) flow rate on oxidation behavior of 625 alloys in the temperature range 900-1000°C showed that by increasing flow rate from 0.5 to 6 m/s, chromium loss increased forming volatile species [88]. The effect of exposure during oxidation on precipitation behavior was also investigated through TEM analysis. Precipitation of embrittling phases during high temperature exposure (600-900°C) is a common problem in most of the austenitic stainless steels, it causes reduction in corrosion resistance and mechanical properties [89, 90]. The different kinds of precipitates reported in literature are χ , σ , δ , M_2N , and $M_{23}C_6$ in high

nitrogen stainless steels [91]. These steels are more prone to nitride precipitation (Cr_2N) [4]. Low nickel, nitrogen stabilized austenitic stainless steel has not been explored for its application in the temperature range of 400-700°C up to 100 h. This chapter deals with the effect of moist airflow on oxidation behavior of Fe-18Cr-21Mn-0.65N austenitic stainless steel from 400-700°C. The oxidized surfaces were characterized using SEM(EDS) and XRD. Mn diffused from the matrix to surface and reacted with the oxygen associated with the passive chromia layer and formed non protective Mn_2O_3 and spinel of the oxides of Fe, Cr and Mn. At 700°C, there was rapid vaporization of Cr and consequent reduction in weight gain in dynamic air (DA) as compared to that in static air (SA). Precipitation of Cr_2N of different morphology was established through TEM analysis.

3.2 Results

3.2.1 Visual Observation

Figure 3.1 shows photographs of the specimens oxidized in static and dynamic humid air conditions at 400-700°C for 100 h. There was difference in the color intensity after oxidation and the oxide scale was thin, compact, and intact in both the conditions.

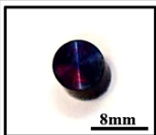
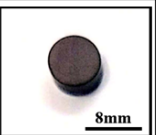
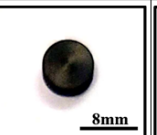

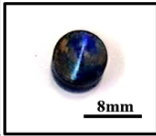
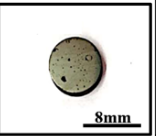
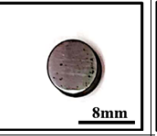
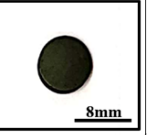
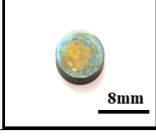


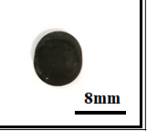
Temperature	400°C	500°C	600°C	700°C
Conditions				
Static Air				
Dynamic Air (2 lpm)				
Dynamic Air (6 lpm)				

Figure 3.1: Photographs of the samples oxidized at 400-700°C for 100 h in static and dynamic air.

3.2.2 Oxidation Kinetics

Figures 3.2 and 3.3 depict oxidation kinetics of the Fe-18Cr-21Mn-0.65N austenitic stainless steel at 400-700°C up to 100 h in static air (SA) and dynamic humid air (DA) condition respectively. The weight gain was less under dynamic air in respect of that in the static air and the decrement in weight gain was more at higher flow rate of 6 lpm than that at 2 lpm (Table 3.2).

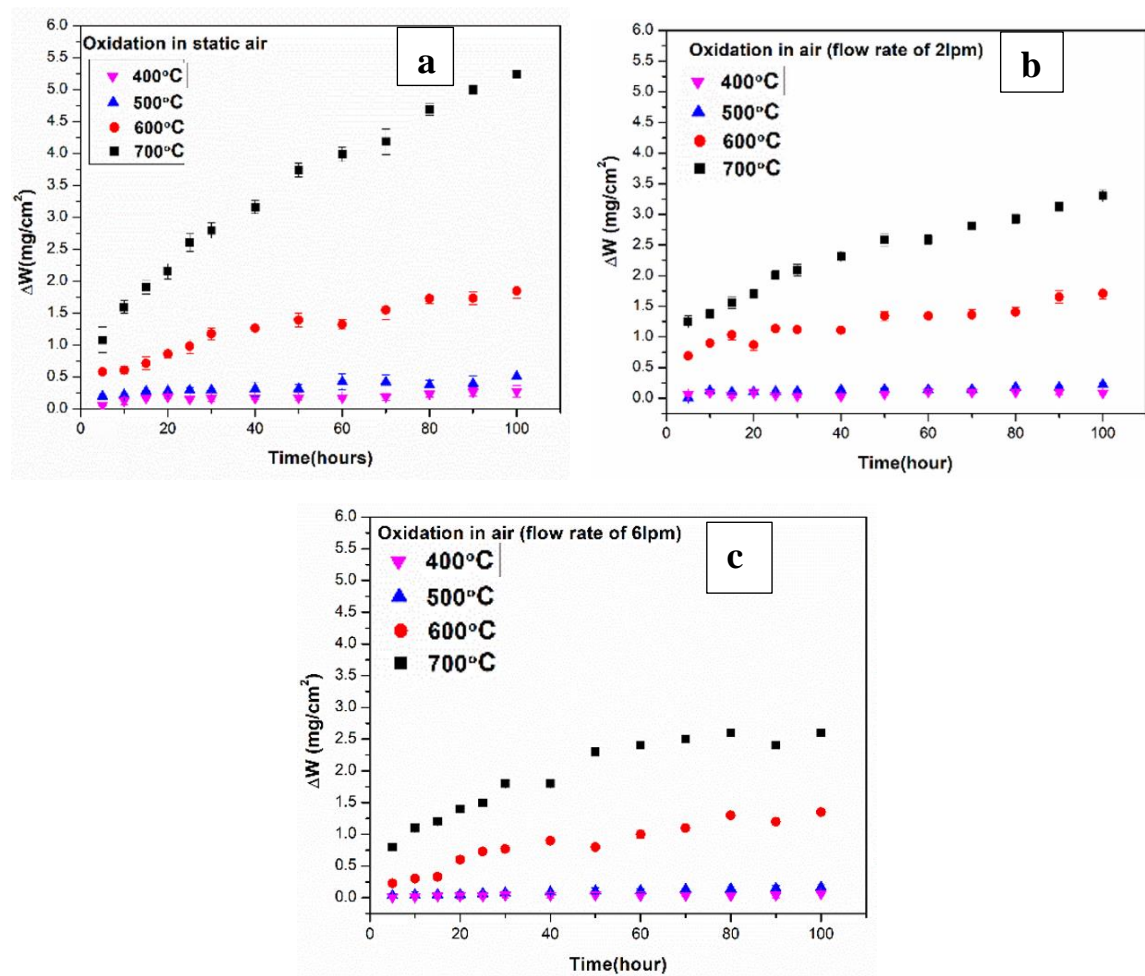


Figure 3.2: ΔW vs time plots for oxidation at 400-700°C up to 100 h in (a) static air, (b) dynamic air-2 lpm, and (c) dynamic air-6 lpm.

Weight gain at 700°C was rapid as compared to those at lower temperatures both in the SA and DA conditions. The exponent (n) was calculated using Equation 3.1 and is shown in Table 3.1. It shows that near parabolic rate law was followed at all the test temperatures in the both SA and DA conditions.

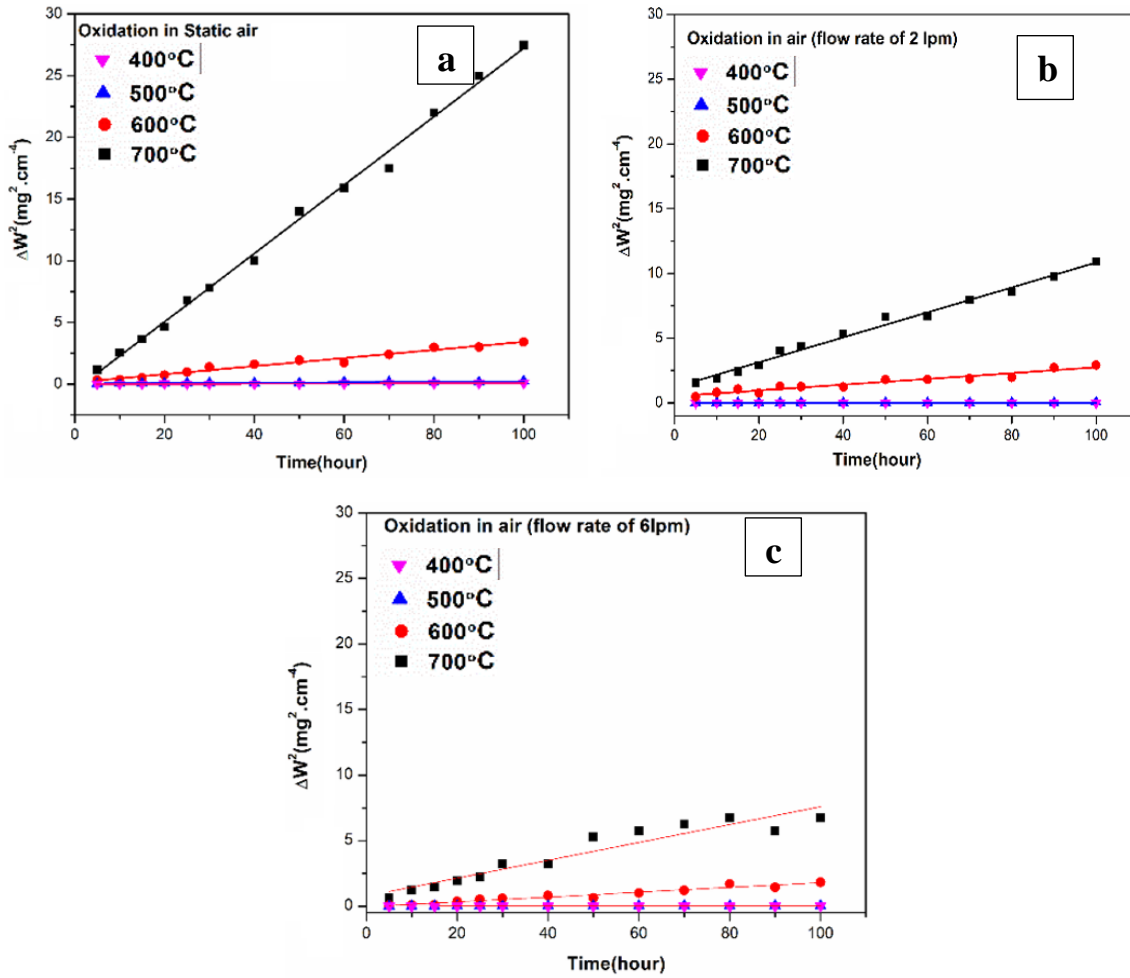


Figure 3.3: ΔW^2 vs time plots for oxidation at 400° to 700°C up to 100 h in (a) static air, (b) dynamic air-2 lpm, and dynamic air-6 lpm.

$$\Delta W^n = kt \tag{3.1}$$

Where ΔW is weight change per unit area (mg/cm^2), n is exponent, k is rate constant in $\text{mg}^2.\text{cm}^{-4}.\text{h}^{-1}$ and t is time of exposure in hour.

Table 3.1: Values of exponent ‘n’.

Temperature (°C)	Static air		Dynamic Air-2lpm		Dynamic air-6lpm	
	n	R ² values	n	R ² values	n	R ² values
400	2.3	0.85	1.6	0.94	2	0.97
500	2.4	0.89	2.1	0.89	1.63	0.94
600	2.3	0.95	2.1	0.85	1.78	0.95
700	1.9	0.99	2.2	0.91	2.40	0.9

The parabolic rate constant (k_p) was determined from the plots of $(\Delta W)^2$ vs time, using the relationship $(\Delta W)^2 = k_p t$ where k_p is parabolic rate constant. The values of k_p are listed in Table 3.2. The activation energy for oxidation was calculated using Equation 3.2.

$$k_p = Ae^{\left(\frac{-Q}{RT}\right)} \tag{3.2}$$

Where k_p is parabolic rate constant in $\text{mg}^2.\text{cm}^{-4}.\text{h}^{-1}$, R is gas constant $8.314 \text{ J}/(\text{mol K})$, T is temperature in Kelvin, A is activation energy constant and Q is activation energy for oxidation. The Arrhenius plot (**Figure 3.4**) clearly shows that the activation energy for SA condition was lower than that for DA condition.

Table 3.2: Weight gain per unit area (ΔW) and parabolic rate constant (k_p).

T (°C)	Weight gain/Area (ΔW) mg/cm^2			Parabolic rate constant(k_p) $\text{mg}^2.\text{cm}^{-4}.\text{h}^{-1}$			R ² Values		
	SA	DA		SA	DA		SA	DA	
		2lpm	6lpm		2lpm	6lpm		2lpm	6lpm
400	0.2±0.09	.08±0.09	.07±0.03	5.5×10^{-4}	4.9×10^{-5}	2.4×10^{-5}	0.90	0.90	0.89
500	0.5±0.1	0.2±0.09	.16±0.03	1.7×10^{-3}	4.1×10^{-4}	2.6×10^{-4}	0.90	0.94	0.98
600	1.8±0.1	1.7±0.03	1.4±0.04	3.5×10^{-2}	2.2×10^{-2}	1.8×10^{-2}	0.96	0.93	0.92
700	5.2±0.1	3.3±0.02	2.7±0.03	2.7×10^{-1}	9.8×10^{-2}	6.8×10^{-2}	0.98	0.98	0.94

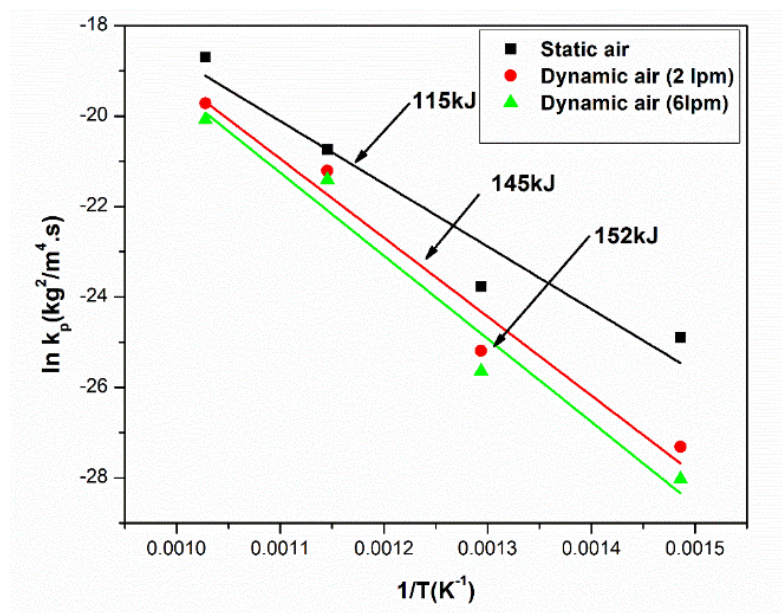


Figure 3.4: Plots for determination of activation energy for oxidation at 400-700°C under Static and Dynamic air conditions.

3.2.3 XRD Analysis

Figure 3.5a and b show XRD patterns of the samples oxidized at 400-700°C up to 100 h in SA and DA condition respectively. The major phases formed after the oxidation are shown in Table 3.3. Ferrite peaks can be seen in both the conditions in the specimens exposed at 500-700°C. At 500°C and above, precipitation of manganese oxide resulted in destabilization of the austenite. It led to formation of ferrite layer on surface of the substrate. The intensity of Mn₂O₃ peak was highest at 700°C. Other phases such as FeMn₂O₄, MnFe₂O₄, and CrFeMnO₄ show low intensity in the specimens exposed at 500-700°C. At 400°C formation of such oxide and spinel was not observed.

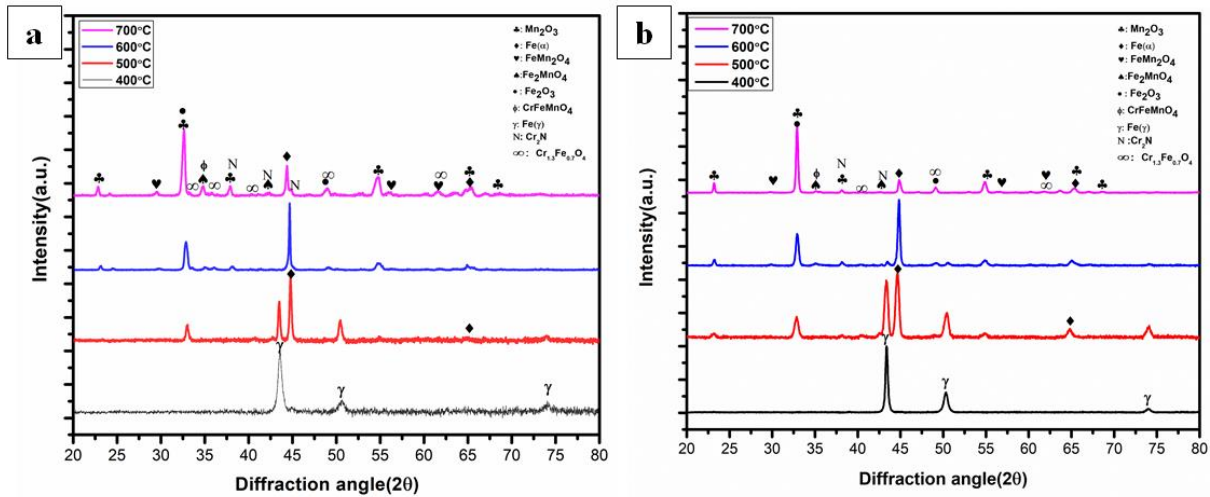


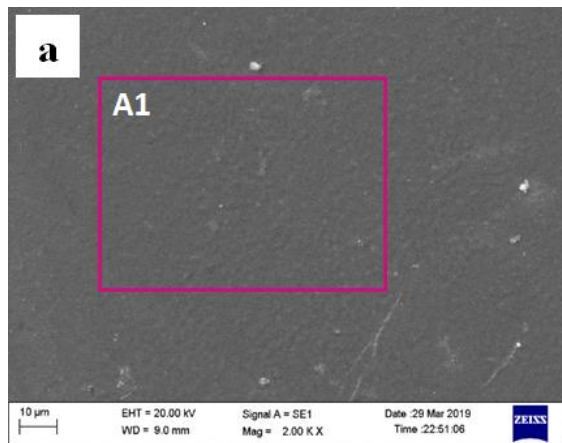
Figure 3.5: XRD patterns of the oxidized Fe-18Cr-21Mn-0.65N austenitic stainless steel at 400-700°C, up to 100 h in (a) static air and (b) dynamic air (6 lpm).

Table 3.3: Phases formed at different temperatures, characterized by XRD.

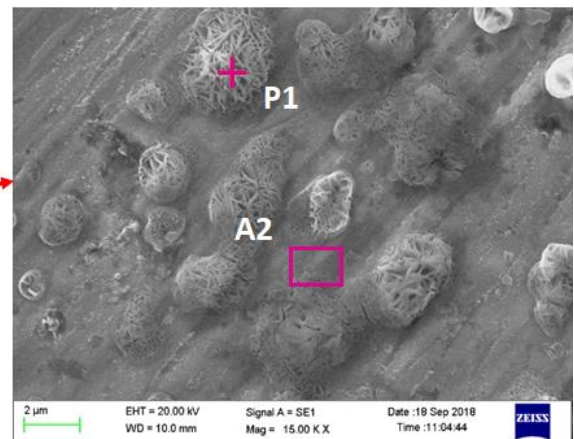
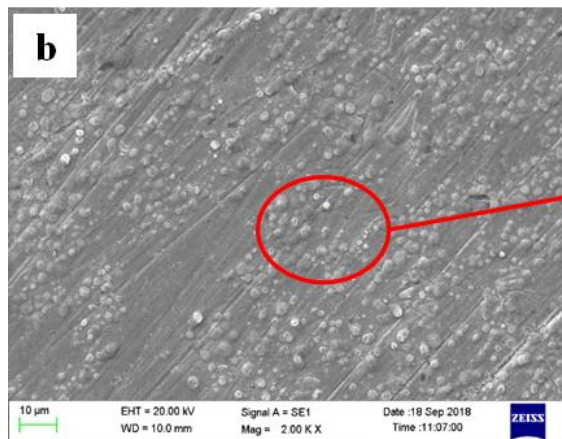
Temperature (°C)	Phases formed	
	DA Condition	SA condition
400	γ	γ
500	Mn ₂ O ₃ , α -Fe, γ, Fe ₂ O ₃ ,	Mn ₂ O ₃ , α -Fe, γ, Fe ₂ O ₃ ,
600	Mn ₂ O ₃ , α -Fe, γ, Fe ₂ O ₃ , Cr ₂ N, CrFeMnO ₄ , Fe ₂ MnO ₄ , FeMn ₂ O ₄ , Cr _{1.3} Fe _{0.7} O ₄	Mn ₂ O ₃ , α -Fe, γ, Fe ₂ O ₃ , Cr ₂ N, CrFeMnO ₄ , Cr _{1.3} Fe _{0.7} O ₄ Fe ₂ MnO ₄ , FeMn ₂ O ₄ ,
700	Mn ₂ O ₃ , α -Fe, γ, Fe ₂ O ₃ , Cr ₂ N, CrFeMnO ₄ , Fe ₂ MnO ₄ , FeMn ₂ O ₄ , Cr _{1.3} Fe _{0.7} O ₄	Mn ₂ O ₃ , α -Fe, γ, Fe ₂ O ₃ , Cr ₂ N, CrFeMnO ₄ , Fe ₂ MnO ₄ , FeMn ₂ O ₄ , Cr _{1.3} Fe _{0.7} O ₄

3.2.4 Morphology of Oxidized Surface and Cross section

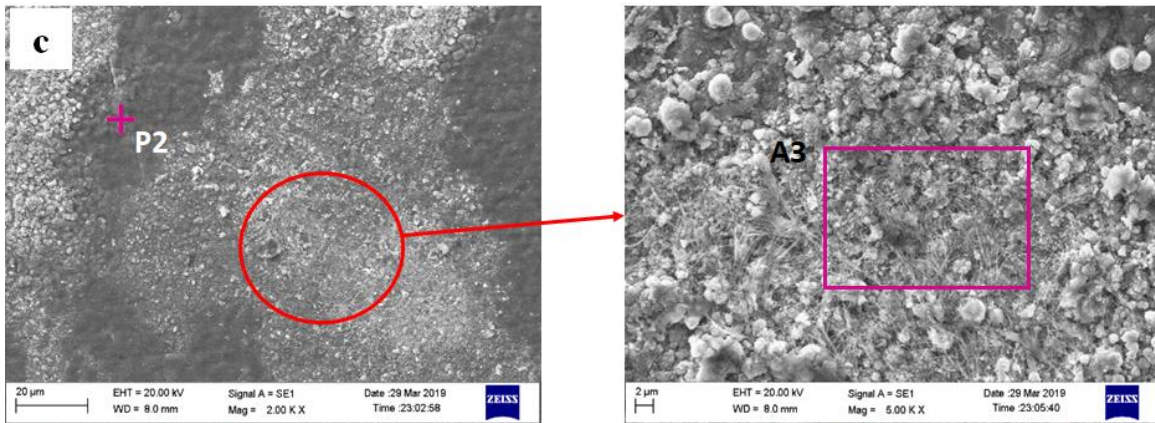
Figures 3.6 and 3.7 show the morphology of oxidized surfaces of the Fe-18Cr-21Mn-0.65N austenitic stainless steel in DA and SA conditions at 400-700°C up to 100 h. Two types of oxide morphology, whiskers and nodules, were observed in both the conditions from exposure at 500-700°C. However, area scan of surface of the sample exposed at 400°C showed less content of oxygen (A1 and A4) without any loss of alloying elements. There was formation of randomly oriented whiskers of spinel of Fe, Cr and Mn oxides on the specimen oxidized at 500°C.



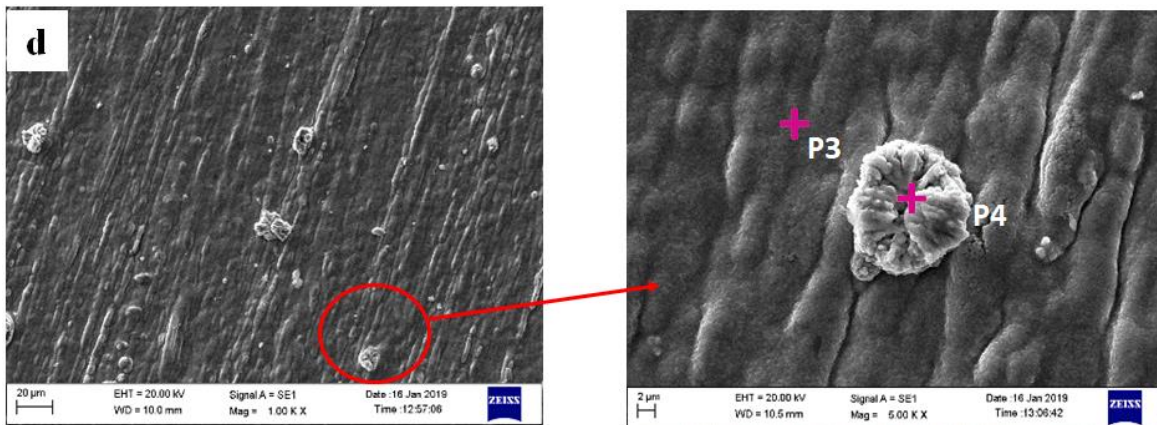
Element	wt%
	A1
Mn	19.47
Fe	54.7
Cr	16.73
O	9.1



Element	wt%	
	P1	A2
Mn	13.31	21.19
Fe	52.24	52.63
Cr	11.07	16.77
O	23.36	9.41



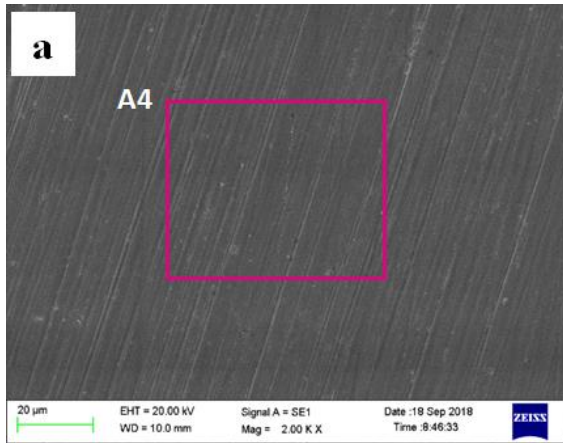
Element	wt%	
	P2	A3
Mn	57.59	47.45
Fe	-	8.4
Cr	12.53	11.34
O	29.87	32.81



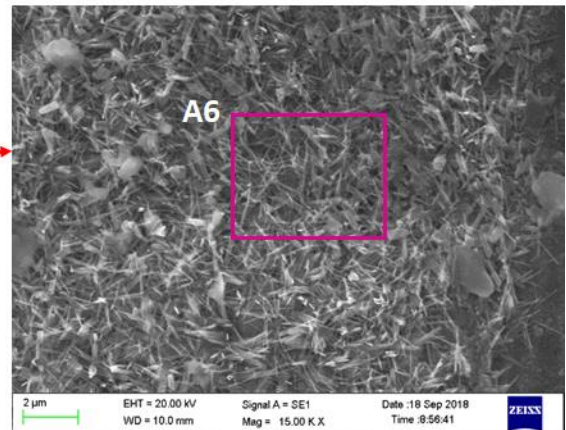
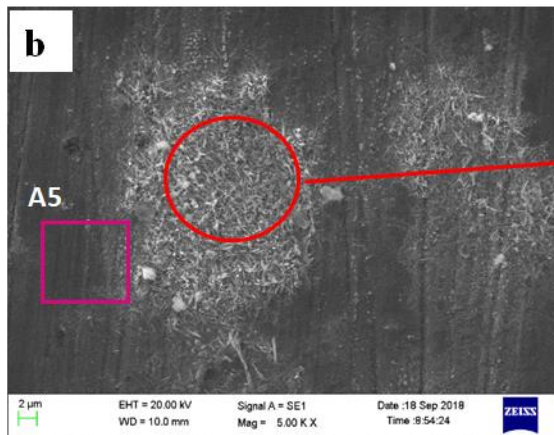
Element	wt%	
	P3	P4
Mn	54.76	75.69
Fe	4.06	-
Cr	9.47	-
O	31.71	24.31

Figure 3.6: SEM micrographs and elemental analysis of the Fe-18Cr-21Mn-0.65N austenitic stainless steel oxidized at (a)400, (b)500, (c)600, and (d)700 °C for 100 h in dynamic air (6 lpm).

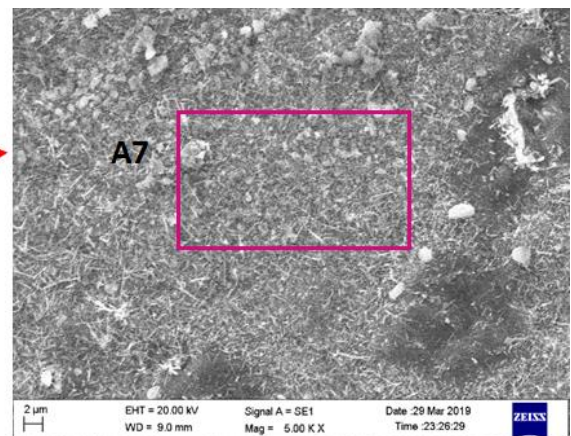
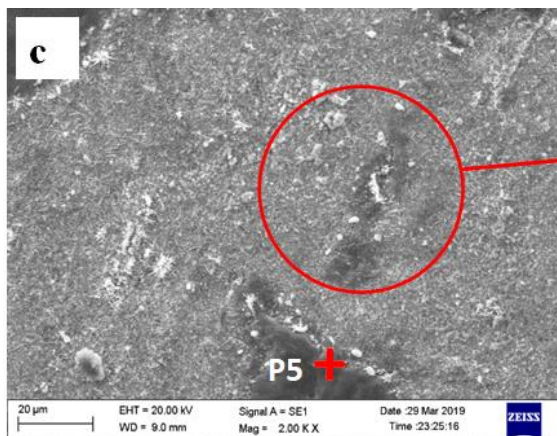
There was increase in the density of whiskers and manganese oxide nodules (A3) on the sample exposed at 600°C. However, whiskers were found to disappear on the surface exposed at 700°C and entire surface was occupied by nodules of manganese oxide (**Figures 3.6 d** and **3.7 d**). Cross section images and EDS area mapping of the steel oxidized in DA and SA conditions at 400-700°C are shown in **Figures 3.8, 3.9, and 3.10** respectively.



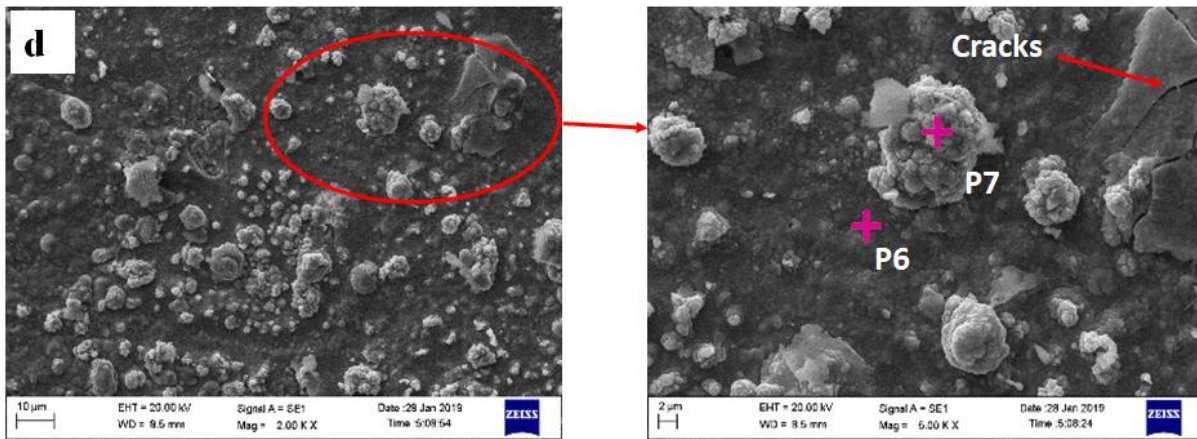
Element	wt %
	A4
Mn	21.43
Fe	56.15
Cr	18.41
O	4.01



Element	wt%	
	A5	A6
Mn	21.71	23.95
Fe	56.82	45.95
Cr	16.93	13.60
O	4.54	16.50

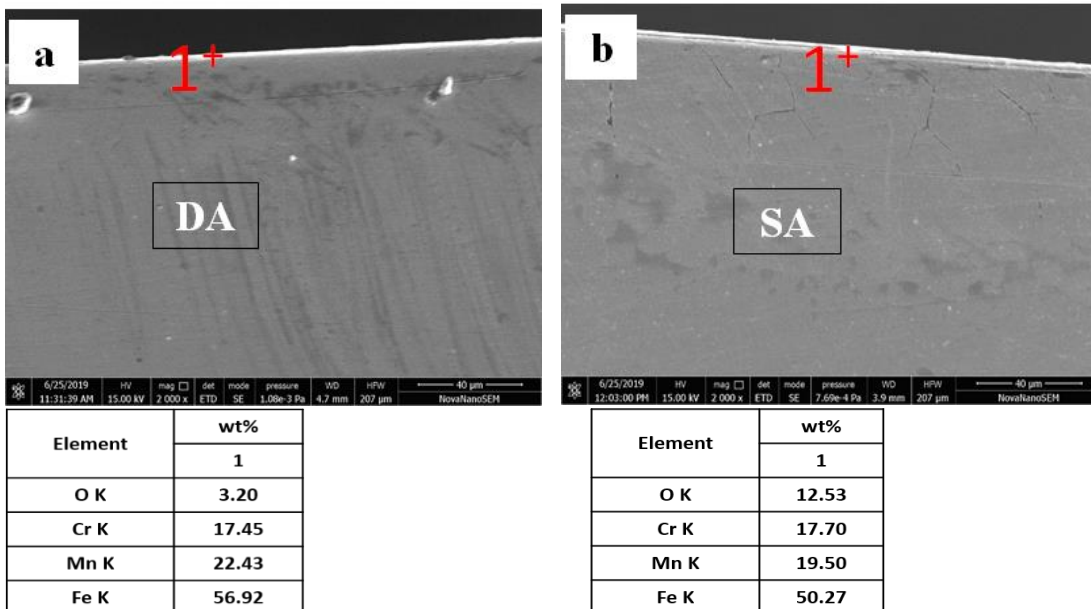


Element	wt%	
	P5	A7
Mn	55.63	47.45
Fe	-	8.4
Cr	11.89	13.34
O	32.48	32.81



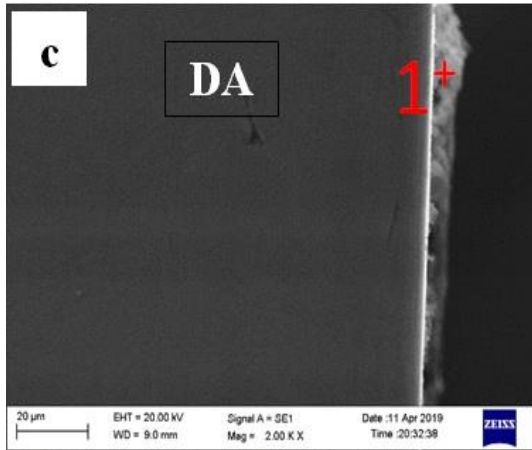
Element	wt%	
	P6	P7
Mn	52.22	59.17
Fe	3.65	2.66
Cr	6.01	5.73
O	28.12	32.44

Figure 3.7: SEM micrographs and elemental analysis of the Fe-18Cr-21Mn-0.65N austenitic stainless steel oxidized at (a) 400°C, (b)500°C, (c), 600°C and (d)700 °C up to 100 h in static air.

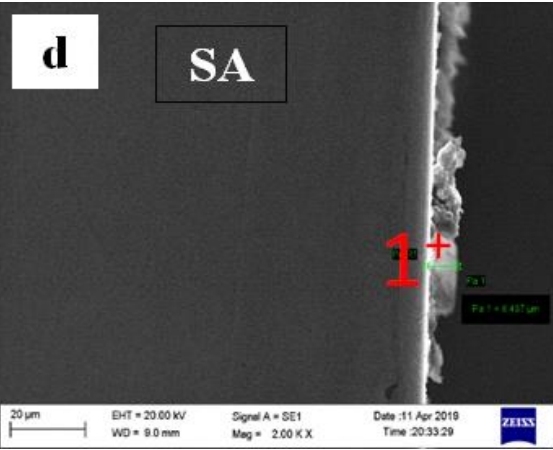


Element	wt%
	1
O K	3.20
Cr K	17.45
Mn K	22.43
Fe K	56.92

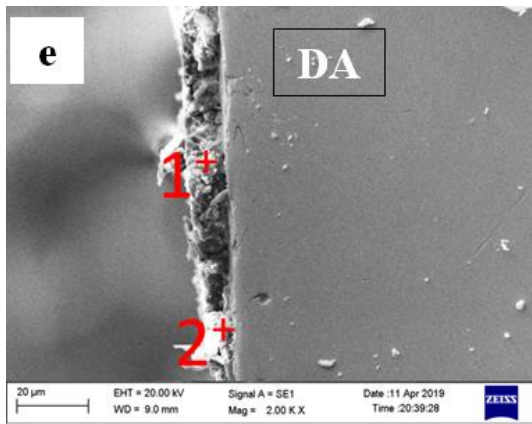
Element	wt%
	1
O K	12.53
Cr K	17.70
Mn K	19.50
Fe K	50.27



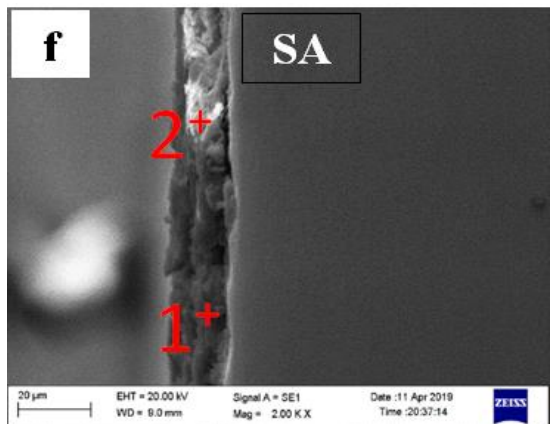
Element	wt%	
	1	
O K	38.96	
Cr K	6.65	
Mn K	17.92	
Fe K	36.47	



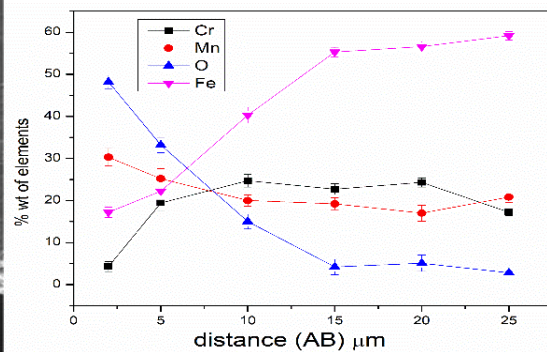
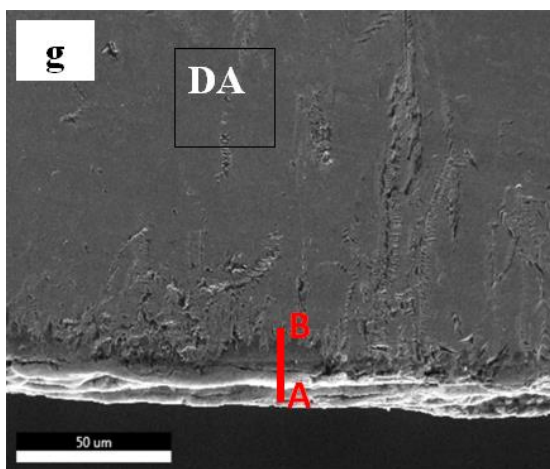
Element	wt%	
	1	
O K	68.75	
Cr K	3.61	
Mn K	9.21	
Fe K	18.43	



Element	wt%	
	1	2
O K	24.46	15.87
Fe K	9.45	32.43
Cr K	6.83	4.49
Mn K	59.26	47.21



Element	wt%	
	1	2
O K	24.43	33.66
Cr K	18.94	17.90
Mn K	20.88	18.68
Fe K	35.40	29.76



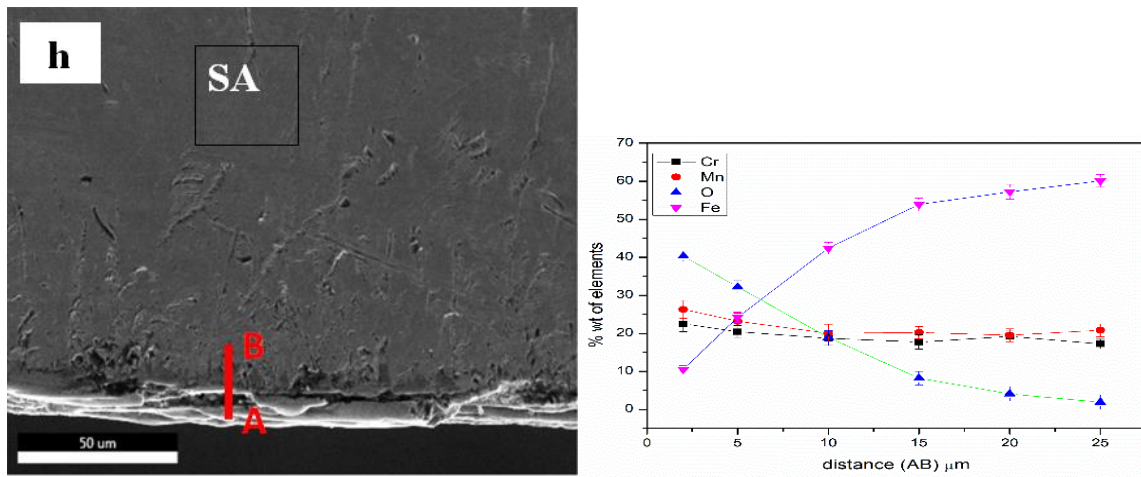


Figure 3.8: SEM-EDS point analysis of cross section of the Fe-18Cr-21Mn-0.65N austenitic stainless steel oxidized up to 100 h at different temperatures; (a, b) 400°C, (c, d) 500°C, (e, f) 600 °C and (g, h) 700 °C in dynamic-6lpm and static air.

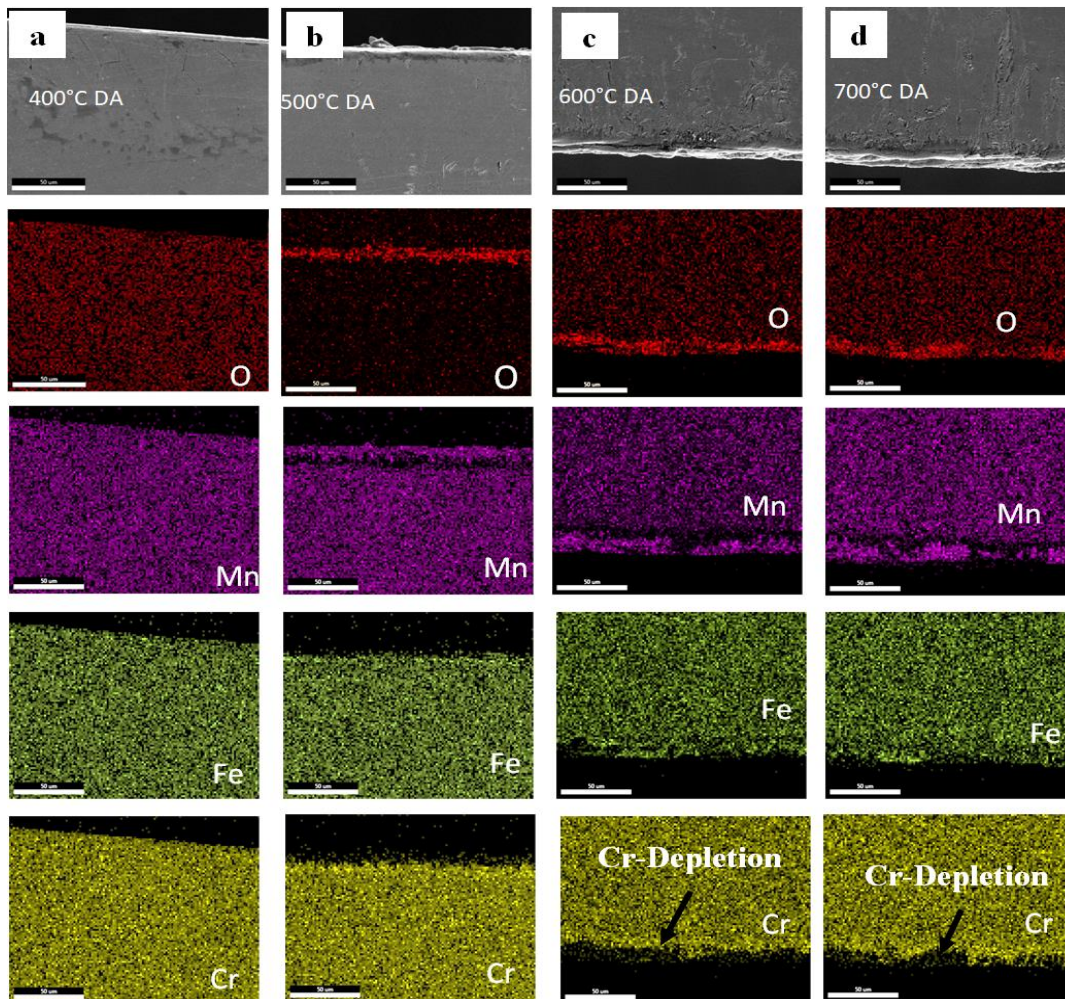


Figure 3.9: EDS mapping of cross section of the Fe-18Cr-21Mn-0.65N austenitic stainless steel oxidized for 100h at: (a)400°C, (b)500°C, (c)600°C and (d)700°C in dynamic air-6 lpm.

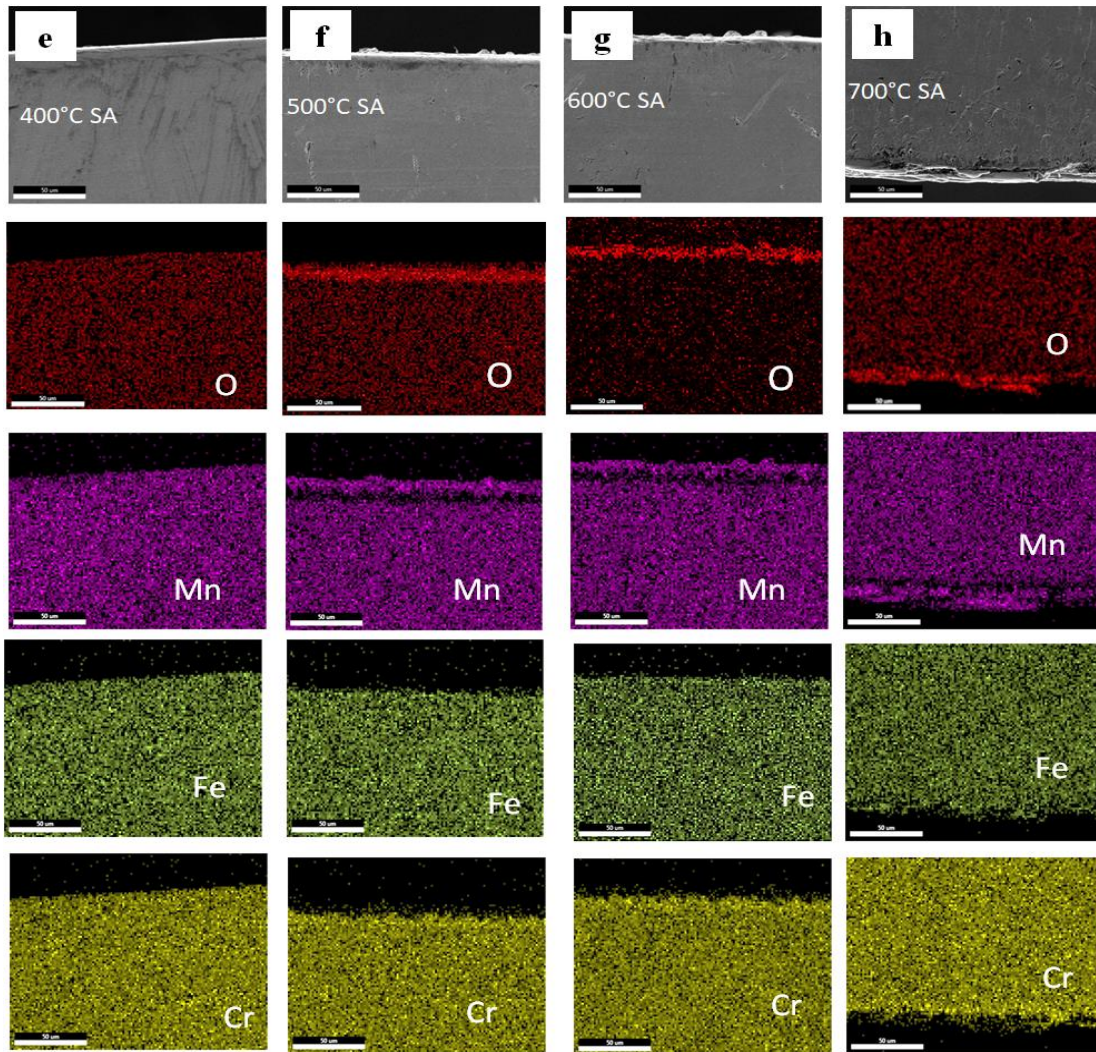
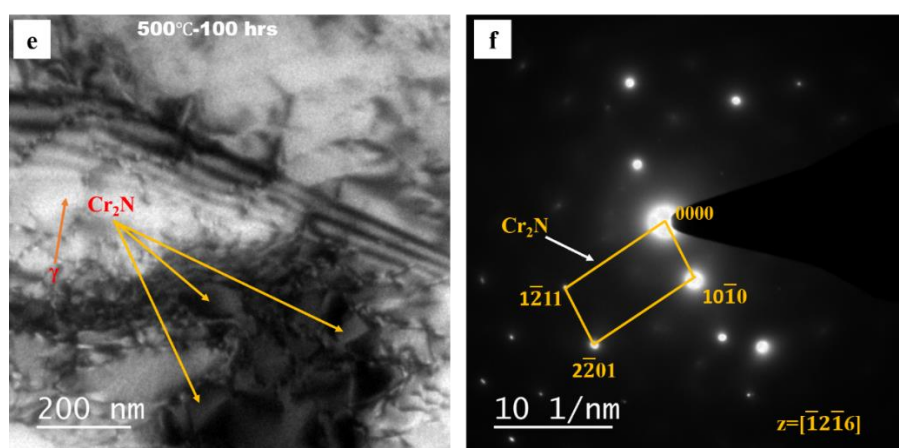
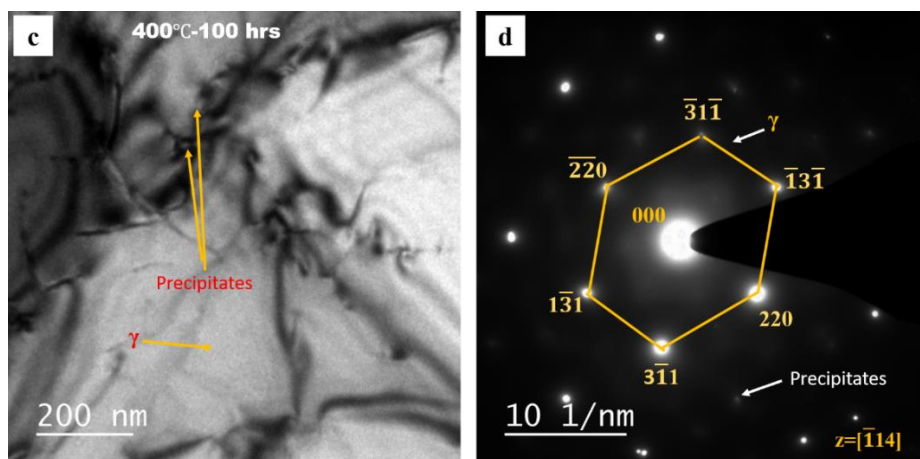
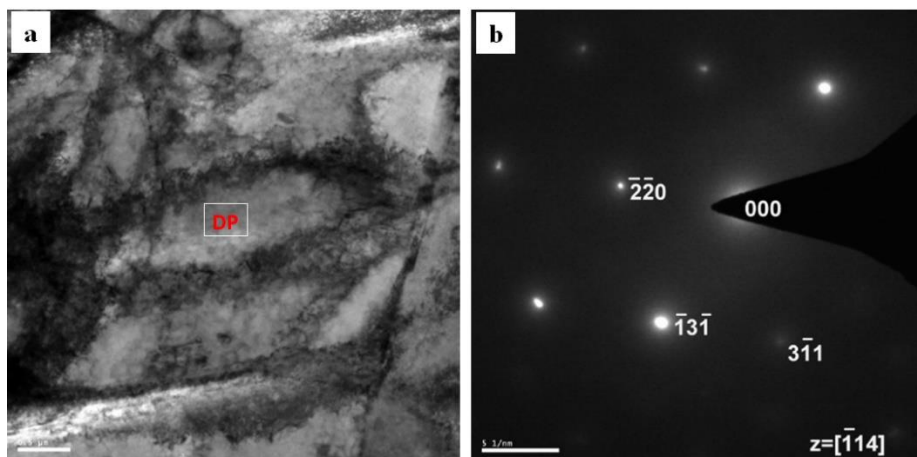


Figure 3.10: EDS mapping of cross section of the, Fe-18Cr-21Mn-0.65N austenitic stainless steel oxidized for 100 h in static air at: (e)400°C, (f)500°C, (g)600°C and (h)700°C.

There is formation of duplex oxide layer consisting of Fe, Cr, Mn and O in the samples oxidized in both conditions above 500°C. It may be noted that Cr content on surface in the SA condition was higher as compared with that of DA condition, that shows that there was loss of chromium in the dynamic airflow condition at 600° and 700°C. There was depletion of manganese from the alloy surface and cracks were there on the top layer (**Figure 3.9** and **3.10**).

3.2.5 Precipitation behavior

Figure 3.11 a shows bright field TEM image and corresponding diffraction pattern (**Figure 11 b**) respectively for the solution treated condition.



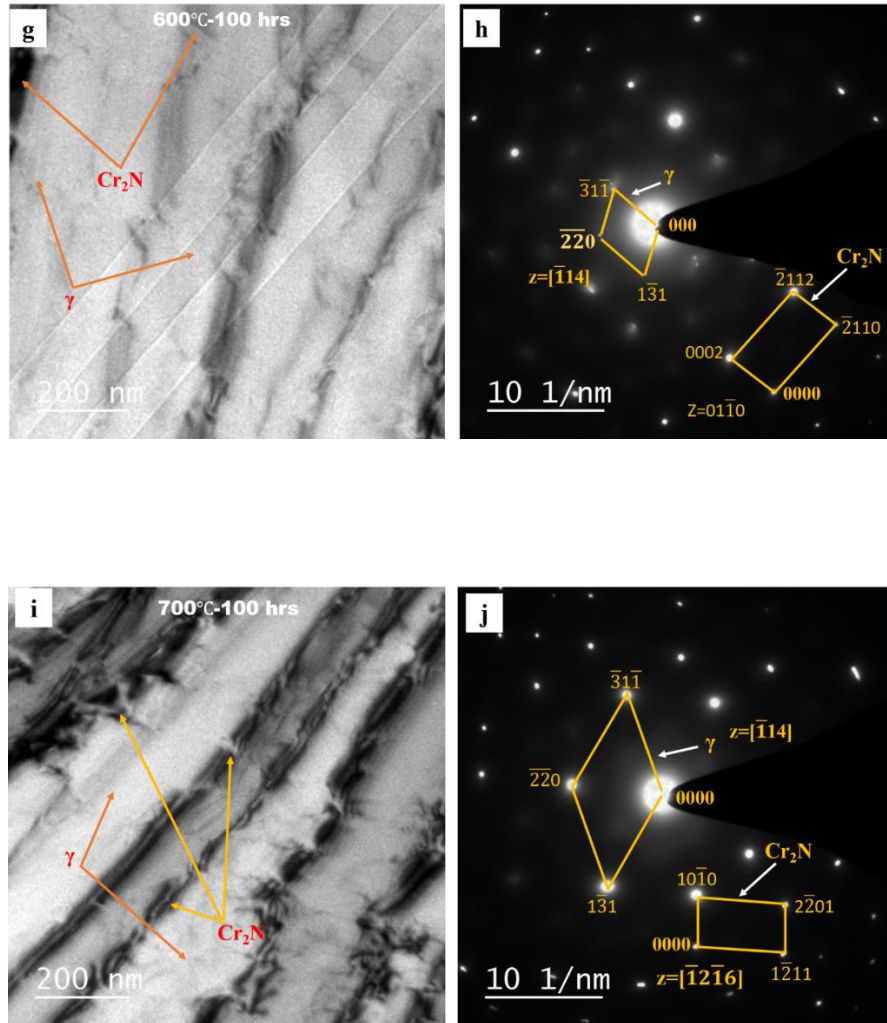


Figure 3.11: TEM bright field images (a, c, e, g) and corresponding diffraction patterns (b, d, f, h) of the samples exposed at 400, 500, 600, and 700°C respectively, up to 100 h.

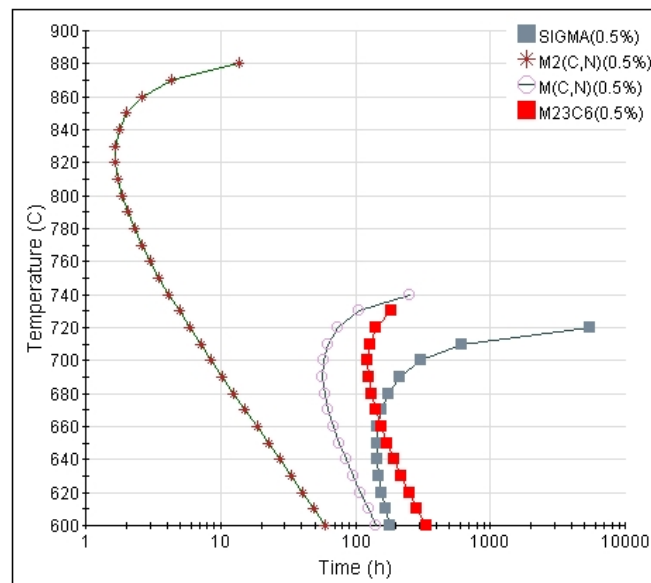


Figure 3.12:TTT diagram of the Fe-18 Cr-21 Mn-0.65 N austenitic stainless steel calculated using J-Mat Pro software.

The diffraction pattern shows austenitic matrix without any precipitate. **Figure 3.11** (c,e,g, i) show bright field TEM image and **Figure 3.11** (d,f,h,j) shows the corresponding diffraction patterns of solution treated samples exposed at 400, 500, 600 and 700°C, respectively up to 100 h. TEM analysis shows that precipitation of Cr₂N was much less in the samples exposed at 400 and 500°C as compared to those exposed to 600° and 700°C after 100 h. The morphology of the Cr₂N precipitate formed at 500°C was faceted whereas there was discontinuous cellular precipitation at 600 and 700°C. **Figure 3.12** shows the Time-Temperature-Transformation (TTT) diagram of the Fe-18Cr-21Mn-0.65N austenitic stainless steel.

3.3 Discussion

3.3.1 Oxidation Behavior

Visual appearance of the samples oxidized in both SA and DA conditions from 400-700°C is seen to be different in color intensity. It is evident that oxidation was more severe in SA condition than that in the DA condition and there was no spallation of oxide scale in any specimen as reported earlier [92]. Weight gain per unit area (ΔW) may be seen to be more in static air than that in dynamic air at 400-700°C. It may be seen that ΔW in DA-6 lpm is less than that in DA-2 lpm. At lower temperatures of 400 and 500°C weight gain is quite insignificant; however, it is much higher at 600°C and particularly at 700°C (**Table 3.2**). The disparity in weight gain between the SA and DA conditions is highest from the exposure at 700°C. It is evident from the linear kinetics plots of ΔW^2 vs time in **Figure 3.4** that near parabolic rate law was exhibited during the oxidation, however, there was much variation in k_p values with temperature of oxidation as reported earlier [92]. Activation energy for oxidation in SA and DA lied from 115-152kJ, comparable to nitrogen bearing steel in SA [35]. However, the higher activation energy for DA based on weight gain, should not be taken as measure of high oxidation resistance in DA because the measured

weight gain was less due to volatilization of Cr. High nitrogen low nickel austenitic stainless steel shows less resistance against high temperature oxidation compared to other austenitic grades and nickel based superalloys [93, 94]. Therefore, high activation energy in DA conditions should not be related to its oxidation resistance.

The XRD and SEM/EDS analyses show that the austenite phase was stable at 400°C in all the conditions after 100 h of exposure. Thus, it is obvious that at 400°C there was no active oxidation and a thin layer of chromia was on the surface because of most negative ΔG of its formation [95, 96]. The surface morphology progressively changed with rise in temperature to 500°C and above, with formation of Mn_2O_3 and Fe_2O_3 nodules (**Figures 3.6 and 3.7**) as observed earlier [97]. Formation of Mn oxide reduces protective ability of the chromia layer and forms spinel together with iron oxide (**Figure 3.13 a**). The mechanism of destabilization of austenite due to formation of Mn oxide is well documented in literatures [35, 86]. Diffusion of Mn through chromia film is much faster than that of Fe and Cr (Table 3.4).

Table 3.4: Diffusion coefficient of cations through chromia layer [98, 99].

Temperature (°C)	Cr (cm ² /s)	Mn(cm ² /s)	Fe(cm ² /s)
400	1.18×10^{-21}	4.64×10^{-22}	1.77×10^{-25}
500	2.27×10^{-20}	2.42×10^{-20}	4.24×10^{-23}
600	2.21×10^{-19}	5.10×10^{-19}	2.90×10^{-21}
700	1.35×10^{-18}	5.74×10^{-18}	8.31×10^{-20}

Formation of Mn_2O_3 results in depletion of Mn at oxide metal interface and favors growth of the BCC α phase [35]. It has been well established that composition of the oxide layer during high temperature oxidation depends on the manganese content of the steel. Even 1% manganese in the alloy diffuses out, reacts with Cr oxide and Fe oxide to form spinel [100]. Higher binding energy of Mn-vacancy pair than Cr-vacancy pair causes faster diffusion of Mn than that of Cr and facilitates formation of $MnCr_2O_4$ and Mn_2O_3 [101, 102]. While the

globules formed in SA (**Figure 3.7 d**) contain also small amount of Fe and Cr, those formed in DA contain exclusively Mn and O (**Figure 3.6 d**).

The relatively less weight gain at 700°C in DA conditions compared with that in SA is associated with loss of chromium (**Figure 3.8 g and h**). The depletion of Cr at 600 and 700°C from the outermost layer may be seen in the elemental mapping of the cross section (**Figure 3.9 d**). The less weight gain in DA than in SA at 700°C in present investigation may be attributed to Cr loss from its volatilization, as volatile $\text{CrO}_2(\text{OH})_2(\text{g})$ resulting from the interaction of Cr associated with Cr_2O_3 and Cr containing spinel with water molecules in flowing air with 95% humidity, in line with earlier reports [103, 104]. As the flow rate increases the weight gain decreases due to increase in the transport of volatile species formed at the surface. Increase in airflow rate washes out the thin stagnant zone of volatile species, present in the diffusion layer near the surface (**Figure 3.13 b**). The volatile species are continuously carried away by the flowing air. The mechanism is well explained by Asteman et al. [103, 105].

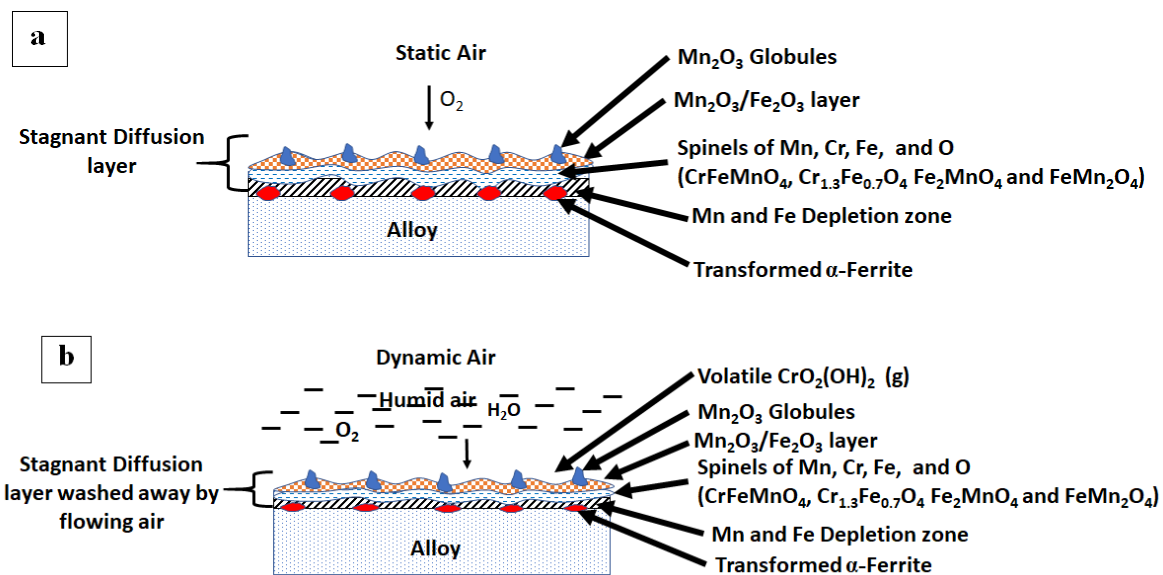


Figure 3.13: Schematic of oxidation mechanism in (a) static and (b) dynamic air at 500-700°C.

3.3.2 Precipitation of Cr₂N

It is evident from the bright field TEM micrograph in **Figure 3.11** that there was only austenite phase in the solution treated condition. Precipitation of chromium nitride (Cr₂N) is more common in nitrogen containing austenitic stainless steel [4]. It may be seen from **Figure 3.11** that precipitation of Cr₂N (0.5wt% Cr₂N) at 700°C starts in < 10 h of exposure. At 600°C, precipitation of Cr₂N takes about 60 h. Precipitation of Cr₂N in the Fe-18Cr-21Mn-0.65N steel at 500-700°C is shown in (**Figure 3.11 e, f, g, h, i and j**). It is interesting to note that precipitation of the σ phase was not observed in the present investigation, that is in line with the TTT diagram (**Figure 3.12**). Depending upon exposure temperature and time, precipitation starts at the grain boundary or within the grains and precipitates are generally of plate/rod/faceted morphology [89, 90]. Cellular/ discontinuous precipitation of Cr₂N starts with increasing exposure time and temperature. At 700°C (**Figure 3.11 i and j**) cellular precipitation of Cr₂N was observed. At 600 and 700°C the morphology of the precipitates was cellular, but at 500°C precipitates had faceted morphology.

3.4 Conclusions

Cyclic oxidation behavior of the Fe-18Cr-21Mn-0.65N was studied for 100 h at 400-700°C in static air and dynamic humid air environment. The rate of oxidation increased with rise in temperature in both the conditions. The high diffusion coefficient of Mn through chromia layer was the key factor in lowering oxidation resistance of this steel. Oxidation from 500-700°C resulted in formation of duplex oxide layer with Mn oxide at the top and spinel CrFeMnO₄, Fe₂MnO₄ and FeMn₂O₄ at the bottom. Evaporation of Cr due to formation of volatile CrO₂(OH)₂ at 700°C, decreased the weight gain in humid dynamic air condition as compared to that in static air. TEM study showed cellular precipitation of HCP chromium nitride (Cr₂N) at 600 and 700°C while at 500°C faceted globular morphology was observed. Precipitation of the detrimental σ phase was not observed in this study.